J. Electr. Electron. Mater.
Vol. 38, No. 5, pp. 469-480 September 2025
doi: https://doi.org/10.4313/JEEM.2025.38.5.2
ISSN 1226-7945(Print), 2288-3258(Online)

Flexible Thermoelectric Materials for Wearable Energy Harvesting: Advances in Polymers and Hybrid Architectures

Momanyi Amos Okirigiti[1,2] and Kwi-Il Park[1,2,3]

[1]Department of Materials Science and Metallurgical Engineering, Kyungpook National University, Daegu 41566, Korea

[2]Innovative Semiconductor Education and Research Center for Future Mobility, Kyungpook National University, Daegu 41566, Korea

[3]Research Institute of Automotive Parts and Materials, Kyungpook National University, Daegu 41566, Korea

(Received July 2, 2025; Revised July 15, 2025; Accepted July 16, 2025)

Abstract: The rapid evolution of wearable technology has driven a surge in demand for sustainable, self-powered electronic devices. Flexible thermoelectric materials, capable of converting body heat into electricity, have emerged as a promising solution for powering next-generation wearables. This review comprehensively examines recent progress in organic (polymer-based) and hybrid thermoelectric materials, focusing on their design, fabrication, and integration into flexible architectures suitable for conformal contact with human skin. Key developments include advanced doping strategies, post-treatment techniques, and composite engineering, particularly in conductive polymers such as PEDOT: PSS and P3HT, which have significantly enhanced power factors and mechanical flexibility. Additionally, the integration of high-performance inorganic materials into stretchable systems has further elevated device efficiency and durability. The review highlights breakthroughs, ongoing challenges, and future opportunities in realizing practical, scalable, and high-efficiency wearable thermoelectric generators for sustainable energy harvesting applications.

Keywords: Thermoelectric, Flexible, Wearable, Energy harvesting

1. INTRODUCTION

The rapid advancement of technology has significantly accelerated the development of the Internet of Things (IoT), fostering widespread interest in creating flexible and wearable devices. Wearable technology encompasses electronic devices worn as accessories, integrated into clothing, implanted within the body, or applied to the skin. Over the past decade, wearable devices have seen remarkable progress across various domains, including healthcare, medicine, and military applications. Despite their reliability and high bandwidth, batteries remain the primary power source for these portable electronics. However, frequent recharging and replacement pose significant challenges. Consequently, designing a sustainable and efficient self-powered generator to replace bulky charging systems for portable devices has emerged as a critical area of focus [1-3]. In this context, thermoelectric materials emerge as a promising candidate for wearable electronics among energy harvesting technologies, owing to their capacity to convert thermal energy from the human body into electrical energy via the Seebeck effect. The thermoelectric performance of materials is characterized by the dimensionless figure of merit zT, defined as, $zT = \frac{s2\alpha T}{k}$ Where S is the Seebeck coefficient, σ is electrical conductivity, k is thermal conductivity, and T is absolute temperature [4,5].

✉ **Kwi-Il Park; kipark@knu.ac.kr**

Maximizing zT enhances both power generation and energy conversion efficiency in thermoelectric generators (TEGs), as it reflects an optimal synergy between high electrical conductivity and low thermal conductivity, essential for minimizing parasitic heat dissipation while maximizing charge carrier mobility. This relationship underscores the critical balance between electronic transport properties and thermal insulation required for efficient thermal-to-electrical energy conversion [6]. For polymer-based thermoelectric materials, the power factor (PF = $s^2\alpha$) serves as the primary performance metric due to their inherently low thermal conductivity (κ), which diminishes the relevance of the zT. Since polymers typically exhibit minimal heat dissipation, PF, which focuses on the Seebeck coefficient (α) and electrical conductivity (σ), provides a more direct assessment of their ability to convert thermal gradients into electrical energy, bypassing the need to account for negligible κ variations. This approach aligns with polymer-specific advantages such as flexibility and solution processability, while enabling targeted optimization of charge transport properties critical for wearable applications [7-9].

Thermoelectric generators (TEGs) utilize pairs of p-type and n-type semiconductors, where they rely on hole-dominated charge transport and the latter on electron-dominated conduction. To enhance power output, thermoelectric materials are arranged in a configuration that optimizes thermal and electrical connectivity: thermally parallel to maintain a uniform temperature gradient and electrically series to amplify voltage generation [10]. Most traditional rigid TEGs employ brittle inorganic materials; however, wearable applications demand flexible architectures that conform to curved biological surfaces, such as human skin. Due to their pliability, flexible TEG designs have recently predominantly incorporated organic components like conductive polymers (e.g., PEDOT: PSS) and carbon-based composites [11]. However, recent advances have enabled the integration of high-performance inorganic thermoelectrics (e.g., Bi_2Te_3, Ag_2Se, and Sb_2Te_3) into deformable systems through innovative approaches [12]. These include embedding nanostructured inorganic films into elastomeric substrates (e.g., PDMS), creating S-shaped serpentine geometries to accommodate mechanical strain, and utilizing liquid-metal electrodes (e.g., EGaIn) to prevent fracture under repeated bending [13]. Such strategies achieve exceptional flexibility

Fig. 1. Schematic illustration of the flexible thermoelectric materials, fabrication techniques, and expanded application fields.

(e.g., 70% stretchability in Ag_2Se-based devices) while preserving high thermoelectric figures of merit (zT > 0.38 at room temperature) [10]. This paradigm shift from organic to inorganic-dominated flexible TEGs has significantly improved power densities and device efficiencies, owing to the introduction of advanced fabrication techniques, improved flexible material characterization, and expanded application fields, as illustrated in Fig. 1.

This review explores recent progress in flexible thermoelectric polymers for wearable devices, focusing on converting body heat into electricity to enable self-powered electronics. Key advances in material engineering, fabrication methods, and device architectures that optimize thermoelectric performance while ensuring mechanical flexibility are discussed. The review also outlines future challenges and opportunities to realize practical, durable, and scalable wearable thermoelectric generators for sustainable energy harvesting.

2. FLEXIBLE THERMOELECTRIC POLYMERS

Bi_2Te_3-based materials remain the leading thermoelectrics for low-temperature applications near room temperature, particularly in wearable devices, due to their high thermoelectric figure of merit (zT). Nanostructured p-type

$Bi_{0.5}Sb_{1.5}Te_3$ achieves a zT of ~1.4 at 100°C, driven by reduced thermal conductivity through enhanced phonon scattering and a high-power factor (~4,000 μW m^{-1} K^{-2}) [14-16]. For n-type materials, Se-doped Bi_2Te_3 ($Bi_2Se_{0.3}Te_{2.7}$) exhibits a ZT of ~1.0 at 125°C, which decreases to ~0.8 at room temperature due to increased lattice thermal conductivity. While Bi_2Te_3/Sb_2Te_3 superlattices have demonstrated higher zT values at room temperature, their fabrication via epitaxial growth methods is costly and non-scalable, limiting practical adoption [17]. Recent advancements in doping strategies, such as Pb incorporation in $Bi_{0.5}Sb_{1.5}Te_3$, have further optimized carrier mobility and power factors, enhancing room-temperature performance [18].

The conjugated polymer-based thermoelectric (TE) materials have recently garnered significant research interest as alternatives to inorganic semiconductors due to their inherent advantages, including mechanical flexibility, lightweight properties, low-cost manufacturing potential, and solution processability. These materials also exhibit intrinsically low thermal conductivities, a critical parameter for efficient thermoelectric performance, attributed to their disordered molecular structures and phonon-scattering characteristics [19]. Despite these benefits, widespread adoption of polymer-based TE materials has been hindered by their comparatively lower power factors relative to inorganic counterparts, primarily due to limited Seebeck coefficients.

To address these limitations, significant research has focused on optimizing doping strategies, particularly p-type doping through oxidation of polymer backbones, which has enabled electrical conductivities exceeding 1,000 S cm^{-1} in optimized systems [20]. Enhancements in charge carrier mobility, achieved through crystallinity control or the formation of interconnected disordered aggregates with sufficient molecular weight, have further contributed to improved device performance. Nevertheless, the intrinsic trade-off between electrical conductivity and the Seebeck coefficient in doped polymers remains a challenge, as excessive carrier concentrations often suppress Seebeck values below 50 μV K^{-1} [21] underscoring the need for innovative approaches such as density-of-states engineering or hybrid composite design to decouple these interrelated parameters and advance high-ZT polymer thermoelectrics [22].

Within this context, conducting polymers specialized subset of conjugated polymers, have gained prominence as flexible TE due to their tunable electronic properties and mechanical adaptability [20] Key representatives, including polyphenylene vinylene (PPV), polyaniline (PANI), and poly(3,4-ethylenedioxythiophene): polystyrene sulfonate (PEDOT: PSS), are widely studied for their compatibility with solution-based processing techniques, including spin-coating, inkjet printing, and layer-by-layer deposition [20,23]. These materials not only maintain the advantageous low thermal conductivities (0.1–0.4 W/m·K) inherent to conjugated polymers but also achieve moderate to high electrical conductivities, as demonstrated by PANI/single-walled carbon nanotube (SWCNT) composites reaching values up to ~3,500 S/cm. Such developments highlight the ongoing progress in bridging the performance gap with inorganic counterparts, reinforcing the potential of conjugated polymers for next-generation flexible energy harvesting applications [21].

2.1 PEDOT: PSS

PEDOT: PSS is a conductive polymer blend comprising two ionomeric components: poly(3,4-ethylenedioxythiophene) (PEDOT) and poly (styrene sulfonate) (PSS). Its synthesis involves oxidative polymerization, where an aqueous PSS solution is combined with EDOT monomers in the presence of sodium persulfate ($Na_2S_2O_8$) and iron (III) sulfate ($Fe_2(SO_4)_3$) as oxidizing agents. Recent studies highlight the significant impact of composite design and post-treatment strategies on the thermoelectric performance of PEDOT: PSS-based materials. For instance, Dasaroyong Kim et al. [24] demonstrated improved thermoelectric behaviour in polymer composites filled with carbon nanotubes (CNTs) and PEDOT: PSS. The study revealed that the type and concentration of CNTs, the choice of stabilizer, and the drying temperature all significantly influence the enhancement of thermoelectric properties. The attachment of PEDOT: PSS to the CNT bridges provides the tube-tube junctions, thereby facilitating more efficient electron transport within the composite. This electrically conducting PEDOT: PSS network enables electrons to travel more efficiently, resulting in a high electrical conductivity of 40,000 S/m as demonstrated in Fig. 2(a), 2(b).

Solvent post-treatment techniques have been shown to optimize the thermoelectric properties of PEDOT: PSS thin films. Siyao Liu et al. [25] systematically varied the ratios of ethylene glycol (EG) and dimethyl sulfoxide (DMSO) as co-solvents and adjusted treatment temperatures, identifying DMSO as particularly effective at removing insulating PSS due to its high dielectric constant. DMSO-treated films achieved a power factor of up to 28.95 μW m^{-1} K^{-2}, with room-temperature post-treatment depleting PSS and inducing conformational changes in PEDOT that enhanced electrical conductivity without significantly altering its redox state. Building on these findings, Jinji Luo et al. [26] explored additional post-treatment strategies to further boost the thermoelectric performance of PEDOT: PSS films. Their comparative study revealed that DMSO post-treatment was more effective than solution-phase doping, achieving a power factor of 30.1 μW $m^{-1}K^{-2}$ by promoting the formation of elongated PEDOT grains, which improved electrical conductivity while maintaining the Seebeck coefficient. Furthermore, the introduction of 1-ethyl-3-methylimidazolium tetrafluoroborate ($EMIMBF_4$) during post-treatment induced the formation of short, circular PEDOT domains with higher polaron densities. This structural adjustment increased the Seebeck coefficient but slightly reduced conductivity, ultimately yielding a record power factor of 38.46 μW m^{-1} K^{-2} at 50 vol% $EMIMBF_4$.

In parallel with chemical and solvent-based post-treatments, innovative physical processing methods have also shown promise. Bokai Zhang et al. [27] introduced brush printing as a scalable, post-treatment-free approach that leverages shear-induced morphological control. By utilizing meniscus-guided deposition, this method enables precise management of

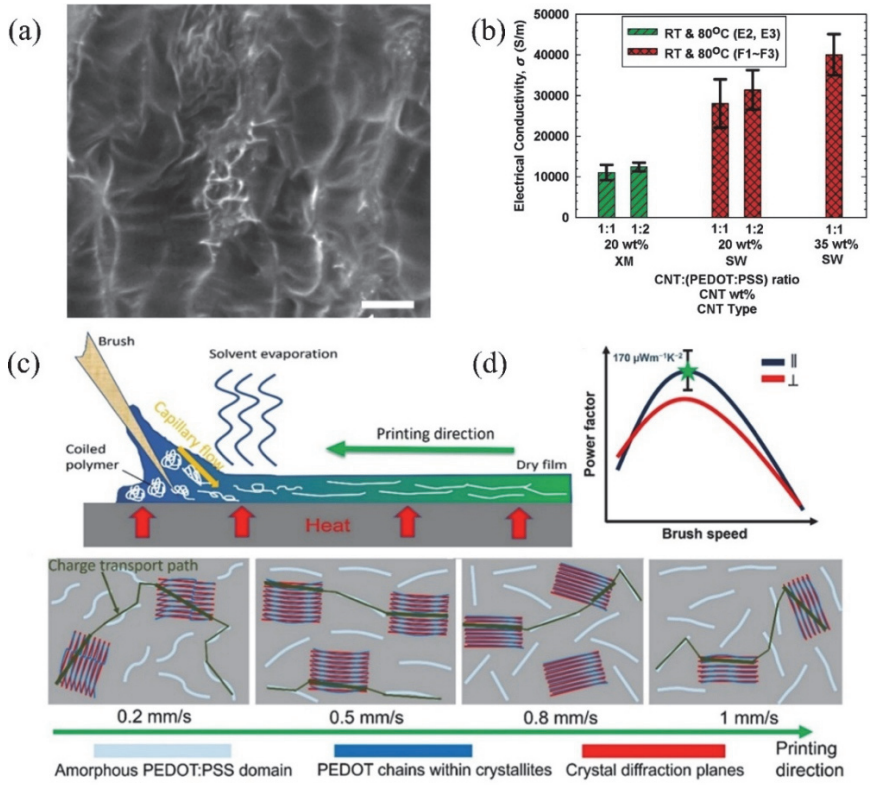

Fig. 2. (a) Illustration of the freeze-fractured cross sections of 9.8 wt% dried at room temperature with a 1:2 ratio of CNT:PEDOT: PSS and (b) electrical conductivities of the composites with XM-CNT and 1:2 ratio between CNT and PEDOT: PSS at room temperature (Reproduced with permission from Ref. [24]. Copyright (2010), ACS Nano). (c) Sketch of stretching polymer chains under the effect of brush printing with full morphology (both crystalline and amorphous phase) of PDEOT: PSS films brushed at different speeds. (d) Power factors change along the parallel and perpendicular direction to printing under different brush speeds (Reproduced with permission from Ref. [27]. Copyright (2025), ACS Applied materials and interfaces).

solvent evaporation and in-situ structural tuning, resulting in extended molecular chains, anisotropic alignment, and enhanced crystalline packing. Such morphological optimizations led to a threefold increase in electrical conductivity (up to 1,900 S cm^{-1}) and a power factor of 170 μW m^{-1} K^{-2}, rivaling those achieved through conventional post-treatment (Fig. 2(c), 2(d)). The dual capability for morphology modulation and direct patterning positions brush printing as a practical and scalable solution for integrating high-performance organic thermoelectric materials into flexible energy harvesting devices.

Complementing these advances, composite engineering has further expanded the performance landscape of PEDOT: PSS-based thermoelectrics. For instance, Vaishali Rathi et al. [28] developed a ternary composite film of PEDOT: PSS, bismuth telluride (Bi_2Te_3), and reduced graphene oxide (rGO), fabricated via spin coating. The synergistic combination of rGO's conductive network, Bi_2Te_3's high thermopower, and PEDOT: PSS's flexibility and phonon-scattering properties resulted in a twelve-fold enhancement in power factor (93.16 μW m^{-1} K^{-2}) over pristine PEDOT: PSS, with a maximum power output of 242.1 nW at $\Delta T = 35$ K.

While these strategies have dramatically improved performance, the long-term stability of modified PEDOT: PSS films remains a critical consideration. Anna Lena Oechsle et al. [29] systematically assessed the thermal stability of ethyl-3-methylimidazolium dicyanamide (EMIM DCA)-treated PEDOT: PSS films. The in-situ analyses revealed that prolonged heating led to morphological degradation and dedoping, which diminished electrical conductivity and overall thermoelectric efficiency. These findings underscore the importance of maintaining controlled operational conditions to preserve the enhanced performance of chemically modified PEDOT: PSS devices. Collectively, these developments illustrate a coherent progression in PEDOT: PSS thermoelectric research, from solvent and chemical post-treatments to advanced printing and composite strategies contributing to the optimization of performance and the realization of flexible, high-efficiency thermoelectric generators.

2.2 P3HT

Poly(3-hexylthiophene) (P3HT) is a conjugated polymer known for its strong tendency to crystallize, efficient hole transport, and widespread use in organic electronics such as solar cells and transistors. Its high crystallinity and hydrophobic nature contribute to its excellent electrical properties and stability in various device applications. Eunhee Lim et al. elucidated the interplay between morphological integrity and charge transport in 2,3,5,6-tetrafluoro-7,7,8,8-tetracyanoquinodimethane (F4TCNQ)-doped poly(3-hexylthiophene) (P3HT) thin films, revealing how structural factors govern nonlinear conductivity dependence on carrier concentration. Resonant soft X-ray scattering demonstrated that vapor-phase F4TCNQ infiltration preserves P3HT's morphology, maintaining crystallite texture, local ordering, and long-range domain connectivity, which are key contributors to enhanced electrical conductivity (Fig. 3(a), 3(b)). While thermopower remains comparable to solution-doped counterparts, vapor-phase doping significantly elevates conductivity, yielding a higher thermoelectric power factor. These findings underscore the critical role of crystallite organization and domain interconnectivity in optimizing doped polymer performance, providing insights into the morphological determinants of charge transport in organic

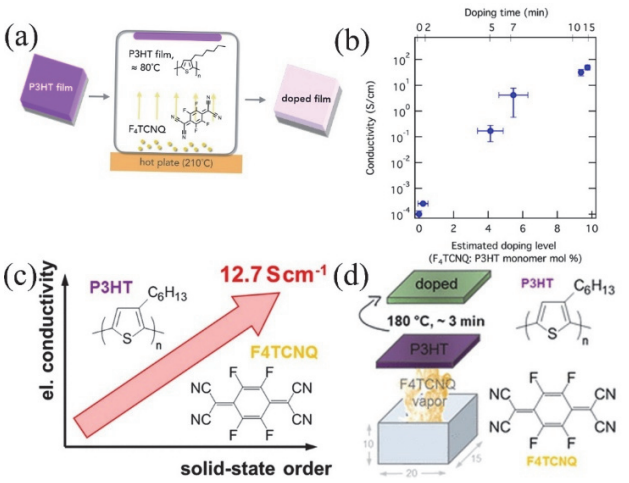

Fig. 3. Illustration of vapor doping method showing the sublimated F_4TCNQ diffusing into the neat P3HT film. (b) Conductivity of P3HT films doped with F4TCNQ via the vapor doping method for varied amounts of time. The estimated doping level is several F4TCNQ monomers per P3HT monomer, calculated from fits of the optical spectra (Reproduced with permission from Ref. [30]. Copyright (2018), Chemistry of Materials). (c) Demonstration of how processing solvent and regioregularity strongly increase electrical conductivity. (d) Schematic of home-built vapor doping chamber that impacts the electrical conductivity of F4TCNQ-doped P3HT (Reproduced with permission from Ref. [31]. Copyright (2017), Macromolecules).

semiconductors [30].

Jonna Hynynen et al. [31] elucidated the role of solid-state order in governing charge transport in F4TCNQ-doped poly(3-hexylthiophene) (P3HT) by decoupling processing and doping effects through vapor-phase infiltration. Their work demonstrated that enhanced crystallinity, modulated via solvent selection and regioregularity optimization, elevates electrical conductivity to 12.7 S cm^{-1} without altering the F4TCNQ anion concentration (~10^{-4} mol cm^{-3}). This improvement stems from a charge-carrier mobility exceeding 10^{-1} cm^2 V^{-1} s^{-1}, driven by long-range connectivity of P3HT crystallites as illustrated in Fig. 3(c), 3(d). Notably, molecular weight exhibited minimal influence on conductivity in doped P3HT, contrasting with undoped systems and underscoring the critical need to reassess structure-property paradigms in strongly doped conjugated polymers [31].

Young Hun Kang et al. [32] demonstrated that gold chloride ($AuCl_3$) doping significantly enhances both electrical conductivity and ambient stability in poly(3-hexylthiophene) (P3HT) thermoelectric films. The coexistence of $AuCl_4^-$ anions and uniformly dispersed Au nanoparticles facilitates efficient charge transport, as confirmed by crystallographic and transmission electron microscopy analyses. $AuCl_3$-doped P3HT achieves a high electrical conductivity of 207 S cm^{-1}, a Seebeck coefficient of 73.9 μV K^{-1}, and an optimized power factor of 110 μW m^{-1} K^{-2}. Crucially, the material retains over 80% of its initial power factor after 300 hours of air exposure, outperforming $FeCl_3$-doped counterparts, which degrade to 20% under similar conditions. A slot-die-coated flexible organic thermoelectric generator (OTEG) fabricated with this composite delivers an open-circuit voltage of 7.96 mV, a short-circuit current of 0.93 μA, and a power density of 18.5 nW cm^{-2} at a 10°C temperature gradient, underscoring its potential for scalable, air-stable energy harvesting applications [32].

2.3 PANI

A study done by Dabin Park et al. [33] demonstrated a flexible polyaniline-coated silver selenide nanowire/polyvinylidene fluoride (PANI-Ag_2Se/PVDF) composite film via a scalable synthesis approach, achieving an optimized power factor of ~196.6 μW m^{-1} K^{-2} at 300 K with

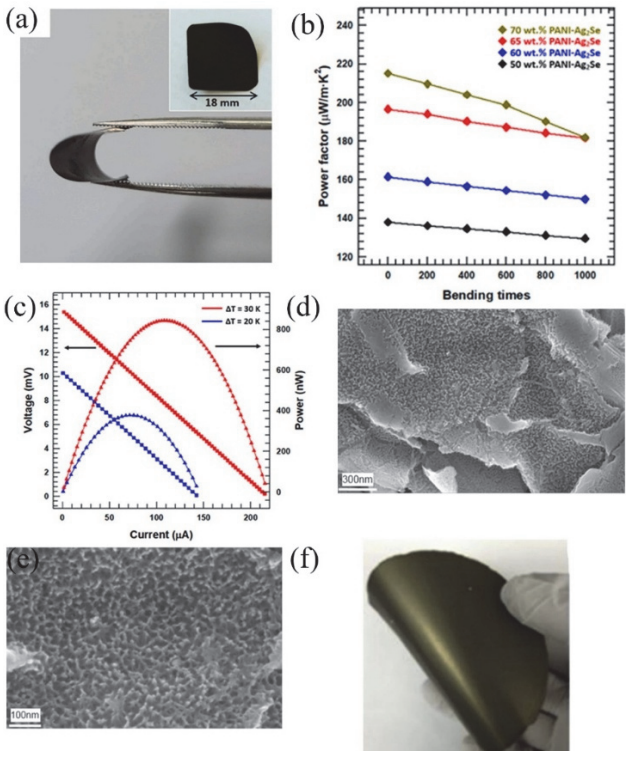

Fig. 4. (a) Digital photograph of composite film at 65% NW. (b) Power factor of the PANI-Ag_2Se/PVDF composite films with various contents of PANI-Ag_2Se. (c) Output voltage and power versus current at ΔT at 20 K and 30 K (Reproduced with permission from Ref. [33]. Copyright (2021), Journal of Alloys and Compounds). (d) Surface morphology of PANI/GNP particles. (e) In situ polymerization of aniline in the presence of GNP particles in 1 M HCL at 0.05 M aniline. (f) Digital photograph showing the flexibility of the final nanocomposite film (Reproduced with permission from Ref. [34]. Copyright (2012), Polymer).

65 wt% nanowire loading. By modulating PANI coating cycles, carrier transport properties were enhanced, while the composite retained 92% of its initial thermoelectric performance after 1,000 bending cycles. A six-leg thermoelectric generator fabricated with this material demonstrated an output voltage of 15.4 mV and a maximum power output of 835.8 nW (power density: ~2.33 W m^{-2}) at ΔT = 30 K, underscoring its potential for wearable energy harvesting as shown in Fig. 4(a)-(c). This work establishes a framework for designing durable, high-performance organic-inorganic hybrid thermoelectric composites through interfacial engineering and Nanostructure Optimization [33]. Jinglei Xiang et al. [34] engineered polyaniline/exfoliated graphene nanoplatelet (PANi/GNP) nanocomposites through in situ

polymerization, leveraging π-π interactions to achieve uniform PANi nanofibril coatings on GNP surfaces. Vacuum filtration of aqueous dispersions yielded paper-like composites, with the Seebeck coefficient peaking at 33 μV K^{-1} for samples containing ~40 wt% PANi and a protonation ratio of 0.2, as illustrated in Fig. 4(d)-(f). The incorporation of GNPs enhanced electrical conductivity to 59 S cm^{-1}, while the nanocomposite's thermoelectric figure of merit (ZT) surpassed its constituents by two orders of magnitude, demonstrating a pronounced synergistic effect between PANi's charge transport and GNP's conductive network. This approach highlights the potential of interfacial engineering in polymer-graphene hybrids for high-performance thermoelectrics [34].

2.4 Organic–inorganic Hybrid Composites

As illustrated in the previous section above, it is evident that the electrical conductivity of the organic TE materials can be increased to over 1,000 Sm^{-1} through the increment of the carrier concentration or enhancing the charge carrier transport. Although their intrinsic low Seebeck coefficient has become the main bottleneck for further promoting their power factor. Therefore, in recent studies, they have demonstrated that the incorporation of inorganic nanostructures into organic TE materials shows great potential in optimizing their power factors. Furthermore, the organic-inorganic hybrid can utilise the advantage of each component largely in enhancing the thermoelectric properties [35].

Y. Wang et al. [36] demonstrated that integrating high-Seebeck-coefficient tellurium nanorods with polyaniline (PANI) to form PANI/Te hybrid films leads to significant improvements in thermoelectric performance due to well-matched nanoscale interfaces that enhance carrier transport while maintaining low thermal conductivity (0.2 W m^{-1} K^{-1}). This synergy enables simultaneous optimization of electrical conductivity, Seebeck coefficient, and thermal conductivity, resulting in a maximum power factor of 105 μW m^{-1} K^{-2} at room temperature and up to 146 μW m^{-1} K^{-2} at 463 K. The ZT value correspondingly increases from 0.156 at room temperature to 0.223 at 390 K, representing the highest reported values for PANI-based thermoelectric materials to date. Utilizing a screen-printing process, the authors fabricated in-plane thermoelectric devices with these hybrid films; a prototype with ten PANI/Te–Ag legs delivered a maximum output voltage of 29.9 mV and power of 0.73 μW at a 40 K temperature gradient [36].

Dabin Park et al. [37] fabricated flexible Ag_2Se nanowire/ PEDOT: PSS composite films with varying Ag_2Se contents (10–80 wt.%) using a straightforward drop-casting technique. By systematically analysing the thermoelectric properties as a function of Ag_2Se loading, they identified that the composite containing 80 wt% Ag_2Se nanowires achieved the highest room-temperature power factor of 178.59 μW m^{-1} K^{-2}. The films also demonstrated excellent mechanical durability, retaining performance after 1,000 bending cycles [37].

Y. Lu et al. [38] introduced a straightforward approach for fabricating high-performance, flexible poly(3,4-ethylenedioxythiophene) (PEDOT)/Ag_2Se/CuAgSe ternary composite films. The process involved in situ synthesis of PEDOT: poly(styrenesulfonate) (PSS)-coated Se nanowires, which served as templates for subsequent formation of

Table 1. A comparison between the thermoelectric properties and performance of various polymers and hybrid materials thin films.

MATERIAL	S (μV. K^{-1})	σ (S.cm^{-1})	$s^2\alpha$ (mW.$m^{-1}K^{-2}$)	
Conductive Polymers				
PEDOT: PSS	9	224	2.3	[47]
PEDOT: PSS(EG+DMSO)	33.4	620	469	[48]
PANI	-	300	-	[49]
PANI: HCL	8	525	-	[50]
PANI: CSA	-	-	$6.3*10^{-2}$	[51]
PPY	-	$2*10^3$	-	[52]
PPY	225	6.7	3.9	[53]
P3HT:PF_6	50	0.8	14	[54]
P3HT:F_4TCNQ	120	400	7	[55]
Hybrid Thermoelectric Composites				
P3HT+BI_2TE_3	90	800	13.6	[56]
PEDOT: PSS+ BI_2TE_3	30	300	119	[57]
PANI +graphene nanosheets	31	237	5.6	[58]
PANI +CNTs and graphene	130	1,000	1825	[59]
PANI+carbon fillers	40	12	20	[60]

PEDOT: PSS-coated Ag_2Se/CuAgSe nanowires. These were then assembled into composite films on porous nylon membranes using vacuum-assisted filtration followed by hot pressing. The optimized composite, featuring hierarchical microstructural defects, achieved a record power factor of approximately 1,603 μW m^{-1} K^{-2} (corresponding to ZT values between 0.6 and 1.05) at 300 the highest reported for organic/inorganic thermoelectric composites to date [38]. A comparative summary of the performances of the thermoelectric polymers and hybrid composites has been presented in Table 1.

3. FABRICATION TECHNIQUES

3.1 Solution-based Processing

Solution-based processing is a cost-effective method for creating high-performance thermoelectric materials. It involves synthesizing controlled nanoparticles or powders in solution, then consolidating them into dense materials with tailored microstructures. This precise control optimizes thermoelectric properties, offering advantages over traditional methods and enabling new manufacturing techniques.

Study conducted by Cheolmin Kim et al. [39] reported the fabrication of flexible thermoelectric composite films by incorporating $Bi_{0.5}Sb_{1.5}Te_3$ (BST) particles into a PEDOT: PSS matrix through a freeze-thawing process followed by drop-casting. The 10 wt% BST/PEDOT: PSS film achieved a power factor of 33.05 μW m^{-1} K^{-2}, far surpassing the performance of BST/poly (vinylidene fluoride) (PVDF) films, which required a much higher BST content (75 wt%) to reach a comparable power factor. This substantial improvement is attributed to the higher electrical conductivity of PEDOT: PSS compared to PVDF. Flexible TEGs based on the PEDOT: PSS composites delivered 25 times greater electrical output than their PVDF-based counterparts. Finite element simulations and practical demonstrations in automotive settings confirmed the device's effectiveness, producing outputs of 4.5 μA and 0.38 mV from body heat (ΔT = 19 K) and 9 μA and 1.8 mV from engine heat (ΔT = 30 K) (Fig. 5(a), 5(b)). These findings underscore the advantage of PEDOT: PSS as a polymer matrix for flexible TE composites, enabling efficient energy harvesting with lower filler content and enhanced real-world applicability.

A report by Da Eun Shin et al. [40] demonstrated a compact, stacked flexible thermoelectric energy harvester (f-TEH) using p- and n-type Bi_2Te_3-PVDF composite films layered with Al foil and PET substrates. Increasing thermoelectric layers (L) enhanced output, with $L = 8$ achieving peak voltage, current, and power. Multiphysics simulations and bending tests validated the design's efficiency and durability, offering a scalable strategy for space-constrained wearable electronics while advancing mechanistic insights into flexible thermoelectric systems (Fig. 5(c), 5 (d)).

Qinggang Wu et al. [11] developed flexible thermoelectric films using SnS and PEDOT: PSS, with optional MWCNTs, via drop-coating. A water-methanol post-treatment boosted conductivity significantly (up to 28.8%), maintaining high power factors (e.g., 43.11 μW m^{-1} K^{-2}). These composite films showed excellent flexibility and were used in functional devices, demonstrating a promising strategy for high-performance wearable energy harvesting.

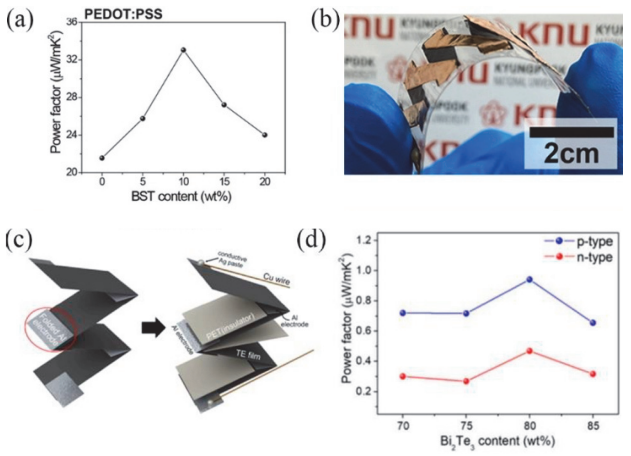

Fig. 5. (a) Power factor of BST/PEDOT: PSS composite films based on the BST concentrations. (b) Photograph of the f-TEG bent by human fingers (Reproduced with permission from Ref. [39]. Copyright (2025), Materials Today Chemistry). (c) Schematic illustration of the fabrication process of Stacked f-TEH. (d) Power factor of the p- and n-type TE films with various ratios of Bi_2Te_3 contents (Reproduced with permission from Ref. [40]. Copyright (2024), ACS Applied Energy Materials).

3.2 Printing Techniques

These techniques offer a set of scalable, cost-effective methods that are used in the fabrication of the thermoelectric materials and devices through the deposition of the functional inks onto the flexible substrates. The most widely utilized method entails screen printing, inkjet printing, and dispenser printing [41]. Screen printing is a versatile technique used for depositing materials onto various substrates, including textiles, electronics, and thermoelectric devices. In this process, a paste or ink is spread across a mesh screen using a blade, and a squeegee then presses the material through patterned openings in the screen, transferring it onto the substrate in the desired design. After the screen is removed, a thin, patterned layer remains on the substrate, ready for further processing.

A study done by Tony Varghese et al. [42] demonstrated a scalable approach to fabricating high-performance flexible thermoelectric films and devices using screen printing of bismuth telluride nanocrystals inks synthesized via a microwave-assisted wet-chemical method. By screen printing these inks onto flexible polyimide substrates, followed by cold compaction and sintering, they produced n-type films with a peak ZT of 0.43-among the highest reported for flexible thermoelectric materials (Fig. 6(a), 6 (b)). The resulting films, several tens of microns thick, maintained excellent flexibility and mechanical durability. A flexible thermoelectric device assembled from these films achieved a high-power density of 4.1 mW/cm² under a 60 °C temperature gradient [42].

According to a study done by Dan Liu et al. [43], they developed a flexible n-type Ag_2Se/polyvinylpyrrolidone (PVP) film using screen printing, systematically examining how varying the Ag_2Se to PVP ratio affects thermoelectric performance. They found that a 30:1 ratio (PI30) yields the best results, with the PI30 film achieving a maximum power factor of 4.3 $\mu W \cdot m^{-1} \cdot K^{-2}$ and maintaining 81% of its original conductivity after 1,500 bending cycles, demonstrating excellent mechanical durability. A flexible thermoelectric generator (F-TEG) fabricated from the PI30 film produced an output voltage of 21.6 mV and a maximum output power of 233.3 nW at a 40 K temperature difference (Fig. 6(c)-(f)). This work highlights that combining PVP with screen printing offers a simple, rapid, and efficient route for producing environmentally friendly, wearable, flexible thermoelectric devices.

Study by Yan Liu et al. [44] developed a scalable inkjet printing approach to fabricate Ag_2Se-based flexible thermoelectric films and devices, enabling precise control over film composition and microstructure by adjusting ink formulations and printing parameters. This method produced large-area, microscale-patterned arrays with (00l) textured features, resulting in an outstanding power factor of 1097 $\mu W\ m^{-1}\ K^{-2}$ at 377 K. The fully inkjet-printed Ag_2Se flexible devices achieved a record-high normalized power output (2 $\mu W\ K^{-2}\ cm^{-2}$) and demonstrated excellent flexibility (Fig. 7(a), 7 (b)).

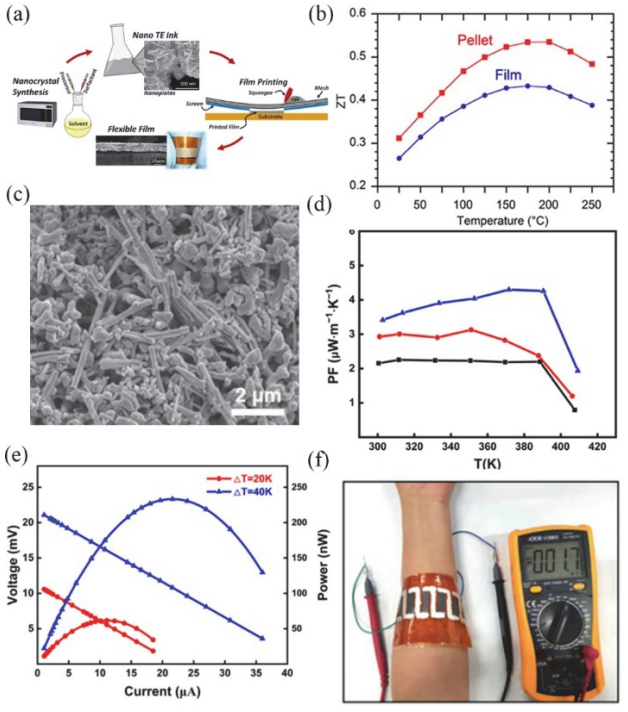

Fig. 6. (a) Schematic demonstration of the fabrication of the nano-crystal synthesis and nano-ink processing using screen printing on flexible substrates. (b) The ZT of a 10 μm-thick flexible film fabricated by printing the nano plate ink (Reproduced with permission from Ref. [42]. Copyright (2016), Scientific Reports). (c) FESEM image of the P130 films. (d) Power factor of the various films (P110, P120, and P130). (e) The relationship between the output voltage, current, and power at ΔT at 20 K and 30 K and (f) the image of 1.7 mV voltage generated by ΔT between the arm and the environment (Reproduced with permission from Ref. [43]. Copyright (2021), Nanomaterials).

Jingjie Du et al. [45] introduced an economical and scalable inkjet printing approach for fabricating high-performance flexible thermoelectric devices using metal chalcogenide nanowires. By employing a template-directed chemical transformation, they synthesized various one-dimensional nanowires (such as Ag_2Te, Cu_7Te_4, and $Bi_2Te_{2.7}Se_{0.3}$), which were dispersed in ethanol to create additive-free inks suitable for inkjet printing. Fully inkjet-printed Ag_2Te-based films demonstrated a power factor of 493.8 $\mu W\ m^{-1}\ K^{-2}$ at 400 K, and the resulting devices achieved a maximum power density of 0.9 $\mu W\ cm^{-2}\ K^{-2}$-both values surpassing those of previously reported inkjet-printed thermoelectrics (Fig. 7(c), 7 (d)). Shih-Yao Chien et al. [46] demonstrated the fabrication of flexible thermoelectric generators (f-TEGs) using dispenser printing, a direct-writing and cost-effective technique. By optimizing the rheology of the printing paste and the sintering process, they achieved high thermoelectric power factors of 23.2 and 19.1 $\mu W/cm \cdot K^2$ for p- and n-type thermoelements, respectively. A planar f-TEG with eight pairs of thermoelements delivered 68 μW of power under a 33 K temperature difference and maintained stable performance after 500 bending cycles on a 20 mm radius rod.

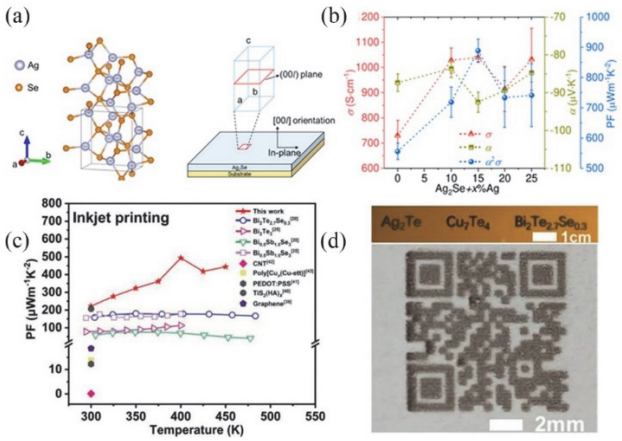

Fig. 7. The crystal structure of the low-temperature β-Ag2Se phase with the film orientation growth. (b) Room temperature Seebeck coefficient, electrical conductivity, and the power factor as a function of Ag ink content (Reproduced with permission from Ref. [44]. Copyright (2021), Nanomaterials). (c) Power factor of various thermoelectric films prepared by inkjet printing. (d) Digital photograph of inkjet-printed patterns (Reproduced with permission from Ref. [45]. Copyright (2021), Nanomaterials).

4. CONCLUSION AND FUTURE OUTLOOK

Flexible thermoelectric materials and devices are rapidly emerging as promising solutions for powering wearable electronics and distributed sensor networks, thanks to their ability to convert body or ambient heat into electricity. Recent advances in both organic (e.g., PEDOT: PSS, polyaniline) and inorganic (e.g., Bi_2Te_3, Ag_2Se) thermoelectric materials, along with innovative composite and nanostructuring strategies, have significantly improved the power factor and mechanical flexibility of these devices. Scalable fabrication methods such as solution-based processing, inkjet printing, and brush printing have enabled the development of large-area, conformable thermoelectric generators (TEGs) that can be integrated into textiles and skin patches, providing sustainable and continuous power for next-generation wearable technologies. Despite this progress, several challenges remain before flexible thermoelectric devices can achieve widespread practical adoption. Key issues include optimizing the balance between electrical conductivity and the Seebeck coefficient, ensuring long-term mechanical and environmental stability, and developing scalable, cost-effective manufacturing processes. Additionally, the integration of high-performance n-type materials and robust device architectures is crucial for achieving efficient, durable, and high-output flexible TEGs. Addressing these challenges through continued interdisciplinary research will be essential for realizing the full potential of flexible thermoelectric materials in sustainable energy harvesting applications.

ORCID
Kwi-Il Park https://orcid.org/0000-0002-9140-6641

ACKNOWLEDGMENT

This work was supported by the National Research Foundation of Korea (NRF) grant funded by the Korea government (MSIT) (No. RS-2022-NR069105 and No. RS-2024-00403822).

REFERENCES

[1] P. Yadav, N. Dhariwal, A. Sanger, S. B. Kang, and V. Kumar, *Nano Energy*, **135**, 110696 (2025).
doi: https://doi.org/10.1016/j.nanoen.2025.110696

[2] F. Saeedi, R. Ansari, and M. Haghgoo, *Nanostruct. Nano-Objects*, **42**, 101473 (2025).
doi: https://doi.org/10.1016/j.nanoso.2025.101473

[3] N. N. Dao, *Future Gener. Comput. Syst.*, **138**, 172 (2023).
doi: https://doi.org/10.1016/j.future.2022.07.006

[4] J. M. Park, S. Kim, Y. Na, and K. I. Park, *J. Korean Inst. Electr. Electron. Mater. Eng.*, **35**, 119 (2022).
doi: https://doi.org/10.4313/JKEM.2022.35.2.2

[5] D. E. Shin, S. Kwon, S. Y. Bae, J. M. Park, C. M. Kim, and K. I. Park, *J. Korean Inst. Electr. Electron. Mater. Eng.*, **38**, 442 (2025).
doi: https://doi.org/10.4313/JKEM.2025.38.4.14

[6] G. J. Snyder and A. H. Snyder, *Energy Environ. Sci.*, **10**, 2280 (2017).
doi: https://doi.org/10.1039/c7ee02007d

[7] N. Nandihalli, C. J. Liu, and T. Mori, *Nano Energy*, **78**, 105186 (2020).
doi: https://doi.org/10.1016/j.nanoen.2020.105186

[8] S. Xu, X. L. Shi, M. Dargusch, C. Di, J. Zou, and Z. G. Chen, *Prog. Mater. Sci.*, **121**, 100840 (2021).
doi: https://doi.org/10.1016/j.pmatsci.2021.100840

[9] J. Li, A. B. Huckleby, and M. Zhang, *J. Materiomics*, **8**, 204 (2022).
doi: https://doi.org/10.1016/j.jmat.2021.03.013

[10] Y. Mun, S. Park, Y. Kim, W. Park, E. J. Bae, M. Han, Y. H. Kang, J. W. Roh, J. Kim, and K. S. Jang, *ACS Appl. Mater. Interfaces*, **16**, 44841 (2024).
doi: https://doi.org/10.1021/acsami.4c08741

[11] Q. Wu, K. Zha, J. Zhang, J. Zhang, J. Hai, and Z. Lu, *Org. Electron.*, **118**, 106799 (2023).
doi: https://doi.org/10.1016/j.orgel.2023.106799

[12] D. Yang, X. L. Shi, M. Li, M. Nisar, A. Mansoor, S. Chen, Y. Chen, F. Li, H. Ma, G. X. Liang, X. Zhang, W. Liu, P. Fan, Z. Zheng, and Z. G. Chen, *Nat. Commun.*, **15**, 923 (2024).
doi: https://doi.org/10.1038/s41467-024-45092-7

[13] R. Guo, W. Shi, R. Guo, C. Yang, Y. Chen, Y. Wang, D. Cui, D. Liu, and C. Xue, *Nanomaterials*, **14**, 542 (2024).
doi: https://doi.org/10.3390/nano14060542

[14] H. Shang, C. Dun, Y. Deng, T. Li, Z. Gao, L. Xiao, H. Gu, D. J. Singh, Z. Ren, and F. Ding, *J. Mater. Chem. A*, **8**, 4552 (2020).
doi: https://doi.org/10.1039/c9ta13152c

[15] M. Hong, Z. G. Chen, and J. Zou, *Chinese Phys. B*, **27**, 048403 (2018).
doi: https://doi.org/10.1088/1674-1056/27/4/048403

[16] H. Zhu, Z. Deng, Y. Qu, P. He, and H. Geng, *J. Mater. Sci. Technol.*, **232**, 267 (2025).
doi: https://doi.org/10.1016/j.jmst.2024.12.086

[17] S. Wang, G. Tan, W. Xie, G. Zheng, H. Li, J. Yang, and X. Tang, *J. Mater. Chem.*, **22**, 20943 (2012).
doi: https://doi.org/10.1039/c2jm34608g

[18] J. W. Kang, S. M. Hwang, S. Y. Kim, C. Lee, W. S. Seo, S. I. Kim, and H. S. Kim, *J. Korean Inst. Metals Mater.*, **62**, 787 (2024).
doi: https://doi.org/10.3365/KJMM.2024.62.10.787

[19] M. A. Kamarudin, S. R. Sahamir, R. S. Datta, B. D. Long, M. F. Mohd Sabri, and S. Mohd Said, *Sci. World J.*, **2013**, 713640 (2013).
doi: https://doi.org/10.1155/2013/713640

[20] M. A. Shahid, M. M. Rahman, M. T. Hossain, I. Hossain, M. S. Sheikh, M. S. Rahman, N. Uddin, S. W. Donne, and M.I.U. Hoque, *J. Compos. Sci.*, **9**, 42 (2025).
doi: https://doi.org/10.3390/jcs9010042

[21] T. Cao, X. L. Shi, J. Zou, and Z. G. Chen, *Microstructures*, **1**, 2021007 (2021).
doi: https://doi.org/10.20517/microstructures.2021.06

[22] C. J. Yao, H. L. Zhang, and Q. Zhang, *Polymers (Basel)*, **11**, 107 (2019).
doi: https://doi.org/10.3390/polym11010107

[23] E. Song, P. Liu, Y. Lv, E. Wang, and C. Y. Guo, *J. Compos. Sci.*, **8**, 308 (2024).
doi: https://doi.org/10.3390/jcs8080308

[24] D. Kim, Y. Kim, K. Choi, J. C. Grunlan, and C. Yu, *ACS Nano*, **4**, 513 (2010).
doi: https://doi.org/10.1021/nn9013577

[25] S. Liu, H. Deng, Y. Zhao, S. Ren, and Q. Fu, *RSC Adv.*, **5**, 1910 (2015).
doi: https://doi.org/10.1039/c4ra09147g

[26] J. Luo, D. Billep, T. Waechtler, T. Otto, M. Toader, O. Gordan, E. Sheremet, J. Martin, M. Hietschold, D. R. T. Zahn, and T. Gessner, *J. Mater. Chem. A*, **1**, 7576 (2013).
doi: https://doi.org/10.1039/c3ta11209h

[27] B. Zhang, T. Y. Yu, A. Meulemans, V. Naenen, M. Rosenthal, D. Escudero, and F. Molina-Lopez, *ACS Appl. Mater. Interfaces*, **17**, 20236 (2025).
doi: https://doi.org/10.1021/acsami.5c00803

[28] V. Rathi, K. Singh, K. P. S. Parmar, R. K. Brajpuriya, and A. Kumar, *RSC Adv.*, **14**, 34883 (2024).
doi: https://doi.org/10.1039/d4ra06184e

[29] A. L. Oechsle, J. E. Heger, N. Li, S. Yin, S. Bernstorff, and P. Müller-Buschbaum, *ACS Appl. Mater. Interfaces*, **14**, 30802 (2022).
doi: https://doi.org/10.1021/acsami.2c05745

[30] E. Lim, K. A. Peterson, G. M. Su, and M. L. Chabinyc, *Chemistry of Materials*, **30**, 998 (2018).
doi: https://doi.org/10.1021/acs.chemmater.7b04849

[31] J. Hynynen, D. Kiefer, L. Yu, R. Kroon, R. Munir, A. Amassian, M. Kemerink, and C. Müller, *Macromolecules*, **50**, 8140 (2017).

doi: https://doi.org/10.1021/acs.macromol.7b00968
[32] Y. H. Kang, S. J. Ko, M. H. Lee, Y. K. Lee, B. J. Kim, and S. Y. Cho, *Nano Energy*, **82**, 105681 (2021).
doi: https://doi.org/10.1016/j.nanoen.2020.105681
[33] D. Park, M. Kim, and J. Kim, *J. Alloys Compd.*, **884**, 161098 (2021).
doi: https://doi.org/10.1016/j.jallcom.2021.161098
[34] J. Xiang and L. T. Drzal, *Polymer (Guild)*, **53**, 4202 (2012).
doi: https://doi.org/10.1016/j.polymer.2012.07.029
[35] J. Zang, J. Chen, Z. Chen, Y. Li, J. Zhang, T. Song, and B. Sun, *J. Mater. Chem. A*, **9**, 19439 (2021).
doi: https://doi.org/10.1039/d1ta03647e
[36] Y. Wang, S. M. Zhang, and Y. Deng, *J. Mater. Chem. A*, **4**, 3554 (2016).
doi: https://doi.org/10.1039/c6ta01140c
[37] D. Park, M. Kim, and J. Kim, *Polymers (Basel)*, **12**, 2932 (2020).
doi: https://doi.org/10.3390/polym12122932
[38] Y. Lu, Y. Qiu, K. Cai, X. Li, M. Gao, C. Jiang, and J. He, *Mater. Today Phys.*, **14**, 100223 (2020).
doi: https://doi.org/10.1016/j.mtphys.2020.100223
[39] C. M. Kim, S. Kim, N. R. Alluri, B. Bae, M. A. Okirigiti, G. H. Kim, H. J. Park, H. Jang, C. Baek, M. K. Lee, G. J. Lee, and K. Il Park, *Mater. Today Chem.*, **44**, 102532 (2025).
doi: https://doi.org/10.1016/j.mtchem.2025.102532
[40] D. E. Shin, N. R. Alluri, and K. Il Park, *ACS Appl. Energy Mater.*, **7**, 8288 (2024).
doi: https://doi.org/10.1021/acsaem.4c01772
[41] S. E. Yang, H. Han, and J. S. Son, *J. Phys. Energy*, **6** 022003 (2024).
doi: https://doi.org/10.1088/2515-7655/ad3983
[42] T. Varghese, C. Hollar, J. Richardson, N. Kempf, C. Han, P. Gamarachchi, D. Estrada, R. J. Mehta, and Y. Zhang, *Sci. Rep.*, **6**, 33135 (2016).
doi: https://doi.org/10.1038/srep33135
[43] D. Liu, Y. Zhao, Z. Yan, Z. Zhang, Y. Zhang, P. Shi, and C. Xue, *Nanomaterials*, **11**, 2042 (2021).
doi: https://doi.org/10.3390/nano11082042
[44] Y. Liu, Q. Zhang, A. Huang, K. Zhang, S. Wan, H. Chen, Y. Fu, W. Zuo, Y. Wang, X. Cao, L. Wang, U. Lemmer, and W. Jiang, *Nat. Commun.*, **15**, 46183 (2024).
doi: https://doi.org/10.1038/s41467-024-46183-1
[45] J. Du, B. Zhang, M. Jiang, Q. Zhang, K. Zhang, Y. Liu, L. Wang, and W. Jiang, *Adv. Funct. Mater.*, **33**, 2213564 (2023).
doi: https://doi.org/10.1002/adfm.202213564
[46] S. Y. Chien, L. C. Hou, C. C. Li, and C. N. Liao, *Mater. Chem. Phys.*, **287**, 126269 (2022).
doi: https://doi.org/10.1016/j.matchemphys.2022.126269
[47] O. Bubnova, M. Berggren, and X. Crispin, *J. Am. Chem. Soc.*, **134**, 16456 (2012).
doi: https://doi.org/10.1021/ja305188r
[48] G. H. Kim, L. Shao, K. Zhang, and K. P. Pipe, *Nat. Mater.*, **12**, 719 (2013).
doi: https://doi.org/10.1038/nmat3635
[49] S. Bhadra, N. K. Singha, and D. Khastgir, *J. Appl. Polym. Sci.*, **104**, 1900 (2007).
doi: https://doi.org/10.1002/app.25867
[50] J. Li, X. Tang, H. Li, Y. Yan, and Q. Zhang, *Synth. Met.*, **160**, 1153 (2010).
doi: https://doi.org/10.1016/j.synthmet.2010.03.001
[51] C. Nath, A. Kumar, Y. K. Kuo, and G. S. Okram, *Appl. Phys. Lett.*, **105**, 133108 (2014).
doi: https://doi.org/10.1063/1.4897146
[52] S. P. Armes, *Synth. Metals*, **20**, 365 (1987).
doi: https://doi.org/10.1016/0379-6779(87)90833-2
[53] M. Culebras, B. Uriol, C. M. Gómez, and A. Cantarero, *Phys. Chem. Chem. Phys.*, **17**, 15140 (2015).
doi: https://doi.org/10.1039/c5cp01940k
[54] Y. Xuan, X. Liu, S. Desbief, P. Leclère, M. Fahlman, R. Lazzaroni, M. Berggren, J. Cornil, D. Emin, and X. Crispin, *Phys. Rev. B Condens. Matter Mater. Phys.*, **82**, 115454 (2010).
doi: https://doi.org/10.1103/PhysRevB.82.115454
[55] G. Zuo, O. Andersson, H. Abdalla, and M. Kemerink, *Appl. Phys. Lett.*, **112**, 083303 (2018).
doi: https://doi.org/10.1063/1.5016908
[56] M. He, J. Ge, Z. Lin, X. Feng, X. Wang, H. Lu, Y. Yang, and F. Qiu, *Energy Environ. Sci.*, **5**, 8351 (2012).
doi: https://doi.org/10.1039/c2ee21803h
[57] B. Zhang, J. Sun, H. E. Katz, F. Fang, and R. L. Opila, *ACS Appl. Mater. Interfaces*, **2**, 3170 (2010).
doi: https://doi.org/10.1021/am100654p
[58] Y. Du, S. Z. Shen, W. Yang, R. Donelson, K. Cai, and P. S. Casey, *Synth. Met.*, **161**, 2688 (2012).
doi: https://doi.org/10.1016/j.synthmet.2011.09.044
[59] C. Cho, B. Stevens, J. H. Hsu, R. Bureau, D. A. Hagen, O. Regev, C. Yu, and J. C. Grunlan, *Adv. Mater.*, **27**, 2996 (2015).
doi: https://doi.org/10.1002/adma.201405738
[60] C. Meng, C. Liu, and S. Fan, *Adv. Mater.*, **22**, 535 (2010).
doi: https://doi.org/10.1002/adma.200902221